Journal of Asian Ceramic Societies 3 (2015) 123–129

HOSTED BY

Contents lists available at ScienceDirect

Journal of Asian Ceramic Societies

journal homepage: www.elsevier.com/locate/jascer

Thermal cycling behavior and hot corrosion performance of the plasma sprayed $Er_2Si_2O_7$ coatings deposited on C_f/SiC composites

Zuhair S. Khan [a,b], Binglin Zou [b,*,1], Xiaolong Chen [c], Hafiz M. Saleem [a], Tanveer Zia [a], M.B. Khan [a], Xueqiang Cao [b,*]

[a] Center for Energy Systems, National University of Sciences & Technology, Sector H-12, Islamabad, Pakistan
[b] State Key Laboratory of Rare Earth Resources Utilization, Changchun Institute of Applied Chemistry, Chinese Academy of Sciences, Changchun 130022, Jilin, China
[c] State Key Laboratory of Corrosion and Protection, Institute of Metal Research, Chinese Academy of Sciences, Shenyang 110016, China

ARTICLE INFO

Article history:
Received 6 October 2014
Received in revised form 1 December 2014
Accepted 1 December 2014
Available online 18 December 2014

Keywords:
Disilicate
C_f/SiC composites
Microstructure
Thermal cycling
Hot corrosion

ABSTRACT

Rare-earth based disilicates are promising coating materials for C_f/SiC composites. In this study, $Er_2Si_2O_7$ coating was deposited on the C_f/SiC substrate by atmospheric plasma spraying using the solid-state reaction synthesized powders. Sintered $Er_2Si_2O_7$ coupons derived from the synthesized powders were subjected to dilatometric studies showing the average value of 4.3 ppm/°C for the coefficient of thermal expansion. The coated C_f/SiC coupons were thermally cycled between 400 °C and 1500 °C on a burner rig facility until failure of coating. Meanwhile, hot corrosion performance of the free standing plasma sprayed $Er_2Si_2O_7$ coating coupon was evaluated by using molten vanadate salt with loading of 15 mg/cm^2 at 800 °C. Analytical techniques such as X-ray diffraction, scanning electron microscopy and energy dispersive spectroscopy were applied to study the microstructural characteristics of the powders and coatings before and after thermal cycling and hot corrosion tests. Coatings' degradation as a result of thermal cycling and hot corrosion tests was investigated in terms of microstructure and microchemistry transformations.

1. Introduction

As the temperature capability of Ni-based superalloys for the gas turbine applications approaches their intrinsic limit, further improvements in their temperature capability have become increasingly difficult. Therefore, during the recent decades, the emphasis in gas turbine materials developments has also focused on finding suitable structural materials that can possibly replace the Ni-based alloys [1]. It is believed that major improvements in turbine inlet temperatures can be achieved by replacing Ni-based superalloy hot section components with silicon-based ceramic matrix composites (CMCs). Carbon fiber reinforced silicon carbide ceramic matrix (C_f/SiC) composites are among the top candidate materials for various technological applications. They offer several distinct advantages such as high strength and hardness, superior fracture toughness, good thermal shock resistance, high thermal conductivity and low density [2–6]. However, as everything is not perfect, the C_f/SiC composites are unfortunately susceptible to oxidation when subjected to higher temperatures (≥600 °C) in air, causing degradation of its superior properties. The remedial approach to counter such a threat is to use a suitable coating against the oxidation, high temperatures and erosion. Various kinds of protective coatings have been reported recently in literatures [6–8].

Among the various silicon containing ceramics, rare earth silicates such as Re_2SiO_5 and $Re_2Si_2O_7$ (where Re = rare earth element) have been targeted as protective coatings against environments such as those found in gas-turbine engines posing mix of challenges of high temperature and corrosive agents from the fuels. These silicates exhibit many attractive attributes, such as environmental stability, low coefficient of thermal expansion (CTE), chemical stability and good adhesion with Si and SiC containing ceramics. In view of their protective properties, various investigations for rare earth silicates have been devoted to understanding the behaviors at high temperatures and corrosive environments [9,10]. The rare-earth based disilicates are considered promising environmental

* Corresponding authors. Tel.: +86 431 85262285; fax: +86 431 85262285.
E-mail addresses: zoubinglin@ciac.ac.cn (B. Zou), xcao@ciac.ac.cn (X. Cao).
[1] Dr. Binglin Zou is also the first author together with Dr. Zuhair S. Khan.
Peer review under responsibility of The Ceramic Society of Japan and the Korean Ceramic Society.

http://dx.doi.org/10.1016/j.jascer.2014.12.001

and thermal barriers for C_f/SiC as they offer more credentials than monosilicate counterparts, especially when it comes to coefficient of thermal expansion. This in turn can yield a coated C_f/SiC coupon in far less stresses than otherwise coated ones with Re_2SiO_5 coatings. However, this advantage may be realized at some cost as many of the $Re_2Si_2O_7$ have multiple polymorphs having disparities in densities that in turn can spoil the performance of coating in service environments, particularly if the disparity in density is substantial. $Er_2Si_2O_7$, one of the most refractory silicates with a melting temperature of ~1800 °C is a potential candidate for high temperature structural and severe environmental applications. Meanwhile, the CTE of rare-earth based disilicates is reported to be around that of Si or SiC containing ceramic matrix composites. Various efforts were reported in literatures for the rare-earth based monosilicates coatings. However, such coatings with CTE values around 7 ppm/°C are more prone to cracking and thereby delamination from C_f/SiC substrate with the progressing of thermal shock testing. Besides, $Er_2Si_2O_7$ is expected to perform stably in connection to its high oxidation resistance with low evaporation rate and low permeability, etc., thus making it suitable for coating materials for the C_f/SiC composites whose average CTE value from 200 °C to 1500 °C is calculated to be about 2.57 ppm/°C [11].

It should be noted that the performance of plasma sprayed $Er_2Si_2O_7$ coating in extreme environments with temperature up to 1500 °C has not been verified in open literatures. It was widely studied by the optoelectronics community due to its luminescent credentials [12–14]. Belonging to rare-earth disilicates family and owing to its exotic properties, the studies are required to know its usage in the backdrop of hot section components in advanced gas turbine engines used for electric power generation or aerospace propulsion systems. The hot-section engineering components are targeted to be manufactured with CMCs including C_f/SiC, C_f/C and SiC/SiC composites, etc. Such components are not only to tolerate the temperature in the proximity of 1500 °C for enhancing thrust-to-weight ratio but also have to withstand the threats posed by the corrosive impurities generated due to the combustion of the fuels. Such impurities include P_2O_5, V_2O_5, Na_2SO_4, and Na_2CO_3, etc. In order to cope with such severe environmental hazards and thermal loads, the base materials, i.e. CMCs would still have an edge over the conventional engineering materials of Ni-based superalloys. However, the effective usage would only be realized with implication of suitable coatings such as going to be reported in our work.

Various approaches are reported in literatures [15–19] for the synthesis of rare-earth based silicates. They include solid-sate reaction synthese, sol-gel and hydrothermal synthese, etc. In addition, thermal spraying is an widely acceptable route to fabricate the coatings safeguarding the hot-section components for gas turbine applications. Plasma spraying forming relatively dense coating requires feedstock powders to exhibit excellent flow and spherically symmetric powder particle morphologies. The task can be accomplished by the spray drying treatment of the as-synthesized $Er_2Si_2O_7$ powders. It should be mentioned that there have been no data available for the performance of plasma sprayed $Er_2Si_2O_7$ coating at high temperatures on C_f/SiC composites in open literatures. Therefore, a preliminary knowledge of the nature of gradient thermal cycling on a burner rig facility is important, in addition to the hot corrosion behavior of coatings. Therefore, in this work, we have firstly fabricated the $Er_2Si_2O_7$ powders using a conventional solid-state reaction synthesis method and thereby studied its CTE using Dilatometry. The as-fabricated $Er_2Si_2O_7$ powders were plasma sprayed on C_f/SiC composites after the spray drying treatment. The coated C_f/SiC coupon was thermally cycled between 400 °C and 1500 °C on a burner rig setting. In addition, plasma-sprayed freestanding coatings are hot corrosion tested in molten salts containing V_2O_5 at 800 °C.

2. Materials and methods

2.1. Powder fabrication and spray drying treatment

The raw materials used in this study were the commercial powders of Er_2O_3 and SiO_2 with purities >99.9%. Solid-state reaction synthesis and spray drying treatment were done as we reported in a previous study [20]. Herein we briefly describe the main steps involved. The blended powder mixture of SiO_2 and Er_2O_3 with molar ratio of 2:1 was heated in an electric furnace at 1450 °C for 22 h. As a result of this high temperature heat treatment, $Er_2Si_2O_7$ was formed according to the chemical reaction $2SiO_2 + Er_2O_3 = Er_2Si_2O_7$. For the spray drying of as-synthesized product, the ball-mill ground powders were mixed with de-ionized water, gum arabic and tri-ammonium citrate. The obtained suspensions were sprayed into a drying tower (GZ-5, Yangguang Ganzao) in which the water was evaporated and the powders in the liquid droplets were reconstituted to the agglomerate particles with round and/or near round shapes. The agglomerate particles are free-flowing and suitable for atmospheric plasma spraying (APS). Those agglomerate particles with particle size of 50–100 μm were sieved and used as the feedstock powders for APS.

2.2. Atmospheric plasma spraying and gradient thermal cycling on a gas burner rig

The spraying dried powders were plasma sprayed by the Sulzer Metco plasma-spraying unit with F4-MB gun. The main plasma spraying parameters used in this study are listed in Table 1. Thermal cycling performance of the plasma sprayed coating on C_f/SiC substrate was investigated between 400 °C and 1500 °C using a gas torch on a burner rig setting. For each cycle, the coating was heated with surface temperature about 1500 °C for 6 min duration, and then cooled to about 400 °C in 3 min duration. The process was repeated for multiple thermal cycles primarily to see any spallation or debonding of coatings. Infrared radiation pyrometer (λ = 9.6–11.5 μm) was used to monitor the surface temperature of the coating. Few $Er_2Si_2O_7$ coatings with thickness about 400 μm were plasma sprayed on aluminum alloy so that the coatings could be easily peeled off from the substrate for hot corrosion test.

2.3. Hot corrosion test

The freestanding $Er_2Si_2O_7$ coating coupons with uniform sizes of 10 mm × 5 mm × 0.3 mm were prepared by cutting them using a low-speed dicing saw. Now, the freestanding $Er_2Si_2O_7$ coating was hot corrosion tested with V_2O_5 for 6 h at 800 °C with a salt loading of 15 mg/cm^2. For this, the V_2O_5 powder was spread uniformly on the coating surface with a fine glass rod, and the specimens were isothermally heated at the said temperature. Following the said dwell time, the specimens were furnace-cooled down to room temperature.

2.4. Characterization

The fabricated powders and coatings were analyzed using X-ray diffraction for phase identification and optical and scanning electron microscopes for surface morphology. Electron microscopy was mainly carried out by XL-30 FEG, Philips equipped with an EDS and the JSM6460, JEOL. X-ray diffraction studies were carried out by Bruker D8 Advance Diffractometer in Bragg–Brentano geometry with an incident monochromatic Cu Kα radiation with wavelength λ = 1.5406 Å. The operation voltage and current were maintained at 40 kV and 40 mA, respectively. For thermal expansion properties of the as-synthesized compound, Dilatometer DIL 402 C by NETZSCH-Gerätebau GmbH has been used. For this purpose, powders were

Table 1
Plasma spraying parameters for the manufacture of $Er_2Si_2O_7$ coatings.

Spray distance/mm	Voltage/V	Current/A	Plasma gas/SLPM[a]	Carrier gas Ar/SLPM	Powder feed/g/min
110	62	650	Ar = 46, H_2 = 8	2.6	30

[a] SLPM – standard liters per minute.

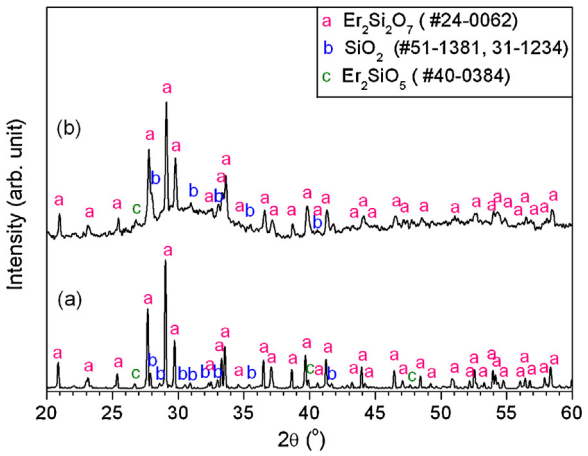

Fig. 1. XRD patterns of (a) $Er_2Si_2O_7$ powders fabricated by solid-state reaction at 1450 °C for 22 h and (b) as-sprayed $Er_2Si_2O_7$ coating deposited on C_f/SiC composites coupon.

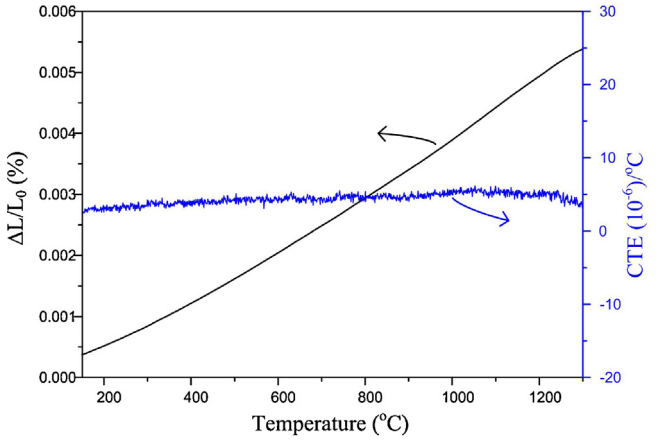

Fig. 2. Variation in the coefficient of thermal expansion (CTE) and thermal expansion rate ($\Delta L/L_0$) with temperature for $Er_2Si_2O_7$ bar by dilatometry. The bar was sintered at 1500 °C for 5 h prior to dilatometric measurements.

cold-pressed into bars with dimensions ($25.3 \times 4 \times 3.5\ mm^3$) suitable for CTE measurements. Prior to CTE measurements, pressed bars were sintered at 1500 °C for 5 h for densification. The CTE measurements were made in air atmosphere from room temperature to 1500 °C. A constant heating rate of 3 °C/min was maintained. Tests are limited in the *X*–*Y* direction, and CTE (α) is calculated by the formula as follows:

$$\alpha = \Delta L/[L(T_0) \cdot \Delta T]$$

where $L(T_0)$ is the length of the sample at the room temperature, $\Delta L = L(T) - L(T_0)$ and $\Delta T = T - T_0$ are the changes of the length of the sample and the temperature, respectively.

3. Results and discussion

3.1. Microstructural and dilatometric evaluations of as-synthesized $Er_2Si_2O_7$ powders

XRD pattern of the as-synthesized $Er_2Si_2O_7$ powders is shown in Fig. 1(a). The crystal structure of $Er_2Si_2O_7$ powders is monoclinic with JCPDS card #24-0062. Some impurity peaks have also been detected originating from the Er_2SiO_5 at 2θ around 26.7°, 39.8°, 47.7° represented by letter "c" and from the SiO_2 represented by letter "b" within the pattern as given by Fig. 1(a). The $Er_2Si_2O_7$ powders exhibited good phase stability for APS because the phase constituent of as-sprayed coating (Fig. 1(b)) is same as that of the $Er_2Si_2O_7$ powders.

Knowledge about thermal properties is important to material development and design. The thermal expansion characteristics of the material in question over a range of temperatures can be useful for selecting and designing different material combinations. This further helps us to predict the material's behavior in high temperature service environments. Fig. 2 shows the thermal expansion behavior of the sintered bar of $Er_2Si_2O_7$ powders, namely the variations in the thermal expansion rate ($\Delta L/L_0$) and CTE with temperature. It can be seen that the value of $\Delta L/L_0$ nearly exhibits a linear increase with temperature increasing from 150 °C to 1300 °C, indicating a continuous volume expansion. The average value of the CTE calculated by the dilatometry data in the CTE curve from 150 °C to 1300 °C is found to be 4.3 ppm/°C, which is in good agreement with the quoted values for rare earth based disilicates for instance in Ref. [19]. $Er_2Si_2O_7$ is found to show rather stable thermal expansion behavior in the tested temperature range. Data during initial 150 °C have been ignored due to instability in the CTE curve owing to the dehydration processes caused by the moist uptake by the specimen prior to testing by Dilatometry. It appears that after 1220 °C, there occurs a minor decline in the CTE value though the average value of CTE from 1220 °C to 1300 °C was quite close to that (i.e. 4.3 ppm/°C) from 150 °C to 1300 °C. Such a trend in the CTE curve of the oxide ceramics may be associated to the lattice distortions, and various mechanisms are proposed for the lattice distortions. Such mechanisms are, for instance, phase transformation, anisotropic thermal expansion within the structure, thermal rocking of atomic polyhedra and transverse motion of oxygen in metal–oxygen–metal linkages [21]. Volume contraction could lead to the decline of CTE; however, there appeared a continuous volume expansion from 1220 °C to 1300 °C. To our understanding, the decline of the CTE beyond 1220 °C could be associated to the lattice distortions which may result from the anisotropic thermal expansions within structure, phase transformation and transverse motion of oxygen in metal–oxygen–metal linkages [21]. Such an explanation for decline of CTE curve was also reported in a previous work [20].

3.2. Microstructure of the as-deposited coatings by plasma spraying

Fig. 3(a) and (b) shows the camera photograph and SEM surface morphology of as-sprayed $Er_2Si_2O_7$ coating on C_f/SiC coupon, respectively. The as-sprayed coatings are found to have different features that formed because of congruent or incongruent melting of the powder particles through plasma flame. The main distinguishable features shown in the SEM image are, for instance, the flattened splats and accumulated incongruent molten media that appears in irregular morphologies after solidification. Fig. 3(c) and (d) shows the EDS spectra and the corresponding quantitative

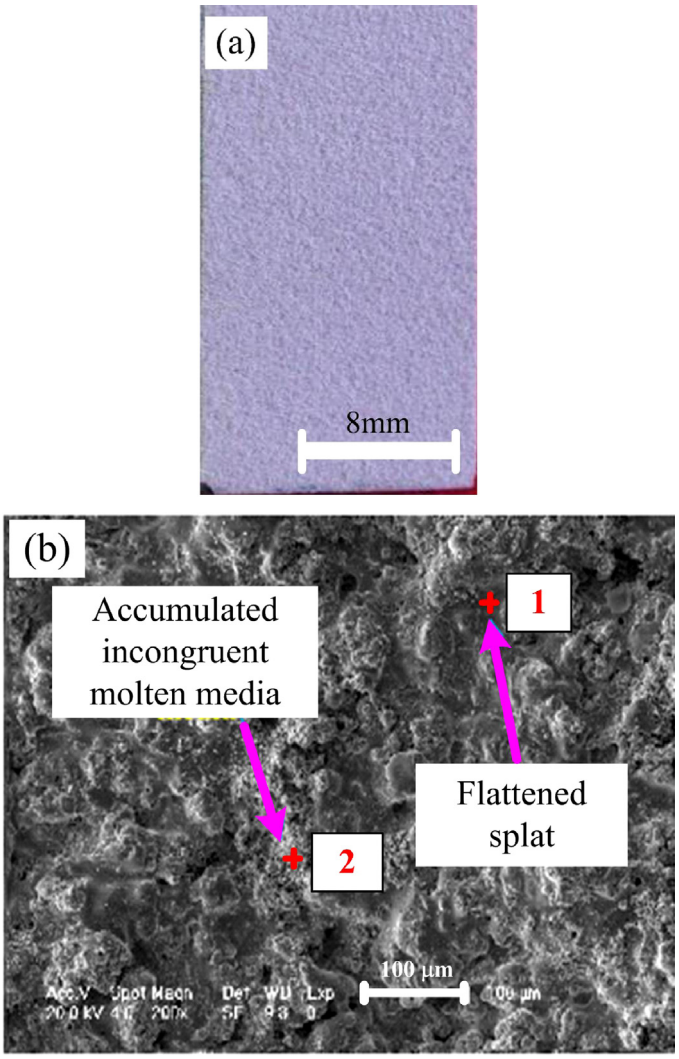

Fig. 3. (a) Macrograph of as-sprayed $Er_2Si_2O_7$ coating on the C_f/SiC coupon, (b) SEM image on the surface of as-sprayed $Er_2Si_2O_7$ coating and (c–d) EDS analysis for point 1 located in the flattened splat and point 2 located in the accumulated incongruent molten media within the as-sprayed $Er_2Si_2O_7$ coating, respectively.

analysis for point 1 located in the flatted splat and point 2 located in the accumulated incongruent molten media (Fig. 3(a)), respectively. The studies reveal that the splats with flat geometries are usually found in relatively higher concentration of silicon in comparison to that found for the accumulated media being irregular in shapes and geometries. On the other hand, erbium is found with the lower percentage in features with flat geometries than that in the irregular features.

Fig. 4(a) shows the cross-section SEM image of the atmospheric plasma sprayed $Er_2Si_2O_7$ coatings on C_f/SiC coupon. It can be seen that the plasma spray processing has resulted in uniform $Er_2Si_2O_7$ coatings with a thickness of ~140 μm on C_f/SiC substrate. The coatings are however found with the presence of pores and microcavities that are usually typical for plasma sprayed coatings. The existence of pores or microdefects may be the result of various factors relevant to the surface state of the substrate or the interface layer and the deposition-related non-uniformities. These factors may be summarized as partially melted particles, small wetting angle of the droplets and short contact time on the substrate/layer due to very large super-cooling rates, differences in the kinetic and viscous energies of the added fluxes, and the possible presence of the absorbed or entrapped gases, etc. [20,22]. Line and point EDS analyses were also performed on coating cross-section for further investigation into the composition profile across the interface. EDS line scan as evident in Fig. 4(b) reveals that the Er and Si are more or less uniformly distributed in the coating cross-section, however, with minor undulation in their composition. The point EDS analyses as given in Fig. 4(c) and (d) depicts that the Er is found in relatively larger proportion close to the interface than that found in the surface of the coating. No major difference was observed for composition of Si in the coating cross-section.

3.3. *Thermal cycling behavior of $Er_2Si_2O_7$ coatings on C_f/SiC*

Thermal shock performance of the plasma sprayed $Er_2Si_2O_7$ coating on C_f/SiC coupon has been evaluated by gradient thermal cycling test with peak temperature of 1500 °C on a gas burner rig facility. Fig. 5(a) and (b) shows the SEM image and the camera photograph of the coating after thermal cycling for 327 times or ~49 h in total. Optical microscopy revealed the presence of cracks in the initial stage of thermal cycling. However, a vivid peeling/spallation with about 5% of the coating's area was found after a total number of 327 cycles as evident in Fig. 5(b). Meanwhile, rest of the coating is found with smoother surface features along with its color that is paler than that for the as-deposited coating.

As stated, the SEM and EDS analyses were performed for the coating thermally cycled for 327 times. The morphology of the coating is characterized by distinct features such as flattened splats as those found in the as-deposited coating, accumulated media and small sponge-like media apparently looking distinct granules. Fig. 5(c)–(e) shows the EDS analysis for point A located in the flattened splat, point B in the accumulated media, and point C in the sponge-like media, respectively. The EDS depicted that the flattened splats are more or less with the same chemical makeup as that for the as-deposited coating. However, the most distinct features are that the sponge-like medias are found to contain quite smaller proportion of Er and larger proportion of silicon (see Fig. 5(e)) as compared to the accumulated media (see Fig. 5(d)).

Fig. 6(a) displays the cross-sectional SEM micrograph of the plasma sprayed $Er_2Si_2O_7$ coatings on C_f/SiC coupon after being subjected to thermal cycling on burner rig facility. The micrograph was of course taken from the region that did not peel off. The complimentary EDS point analyses on cross-section of coating revealed the Er rich surface (Fig. 6(c)) that might have diffused outward from the near interface region of the coating on a high temperature gradient

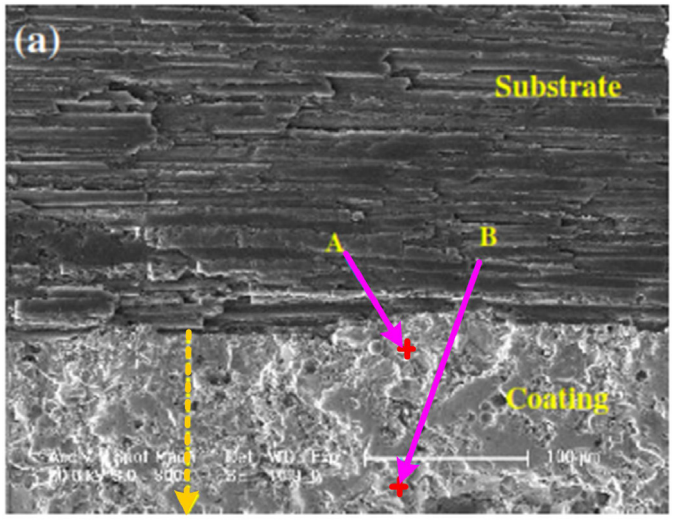

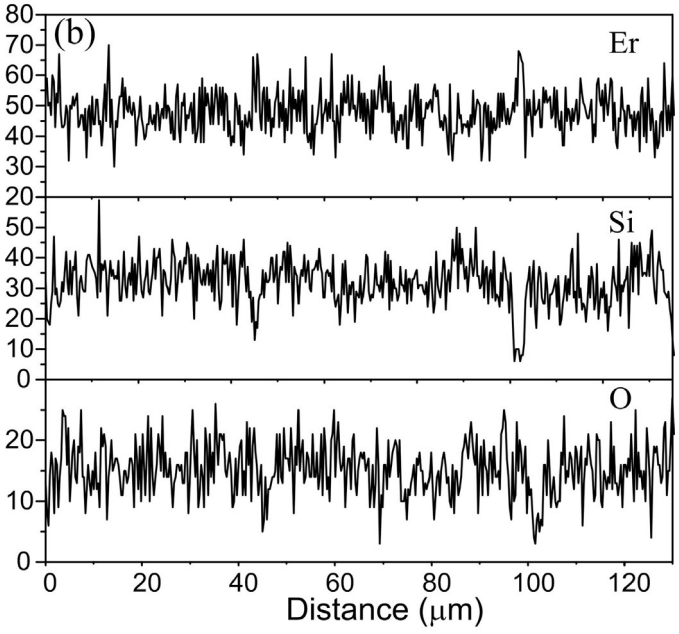

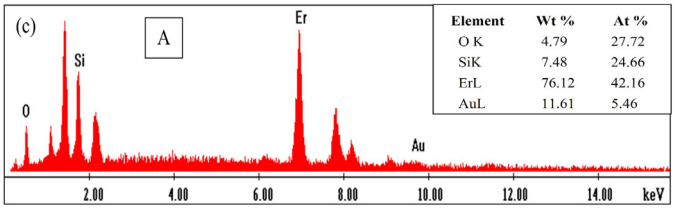

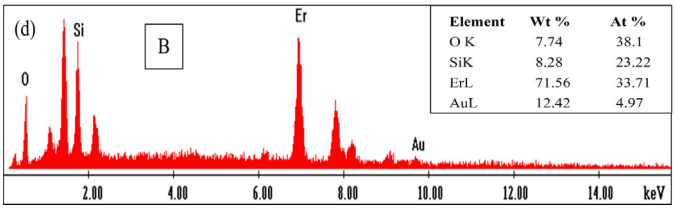

Fig. 4. (a) SEM image on the cross-section of as-sprayed $Er_2Si_2O_7$ coating on C_f/SiC coupon, (b) EDS line scan starting from the interlayer and terminating at the surface of the coating, and (c–d) EDS spectra along with elemental percentages for point A near the interface and point B near the surface of the coating, respectively.

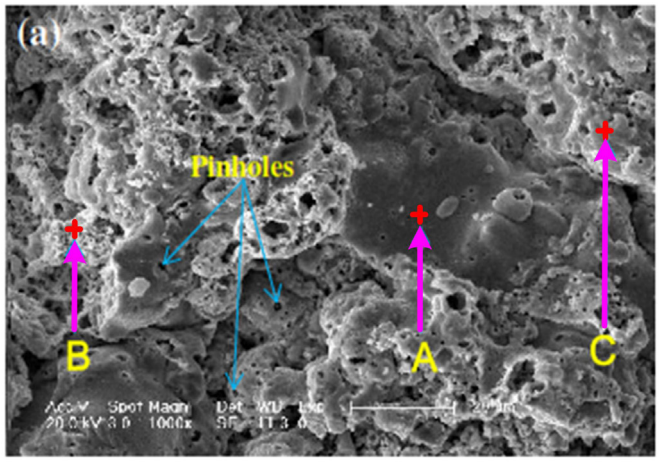

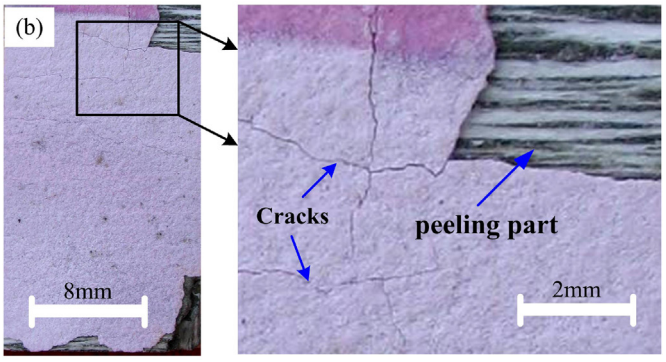

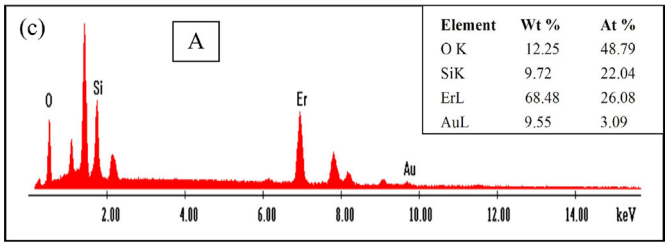

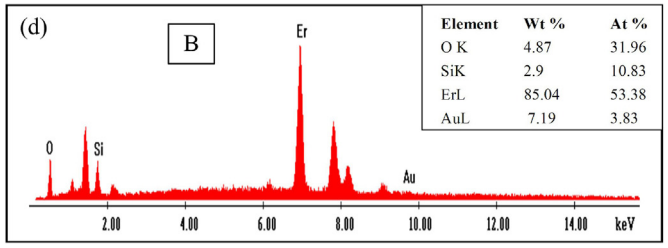

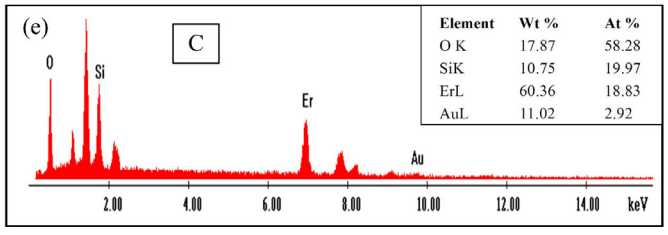

Fig. 5. (a) SEM image on the surface of the thermal shock tested $Er_2Si_2O_7$ coating on C_f/SiC coupon, (b) camera photograph of the thermal shock tested $Er_2Si_2O_7$ coating on C_f/SiC coupon, and (c–e) EDS analysis for point A located in the flattened splat, point B in the accumulated media and point C in the sponge-like media in (a), respectively.

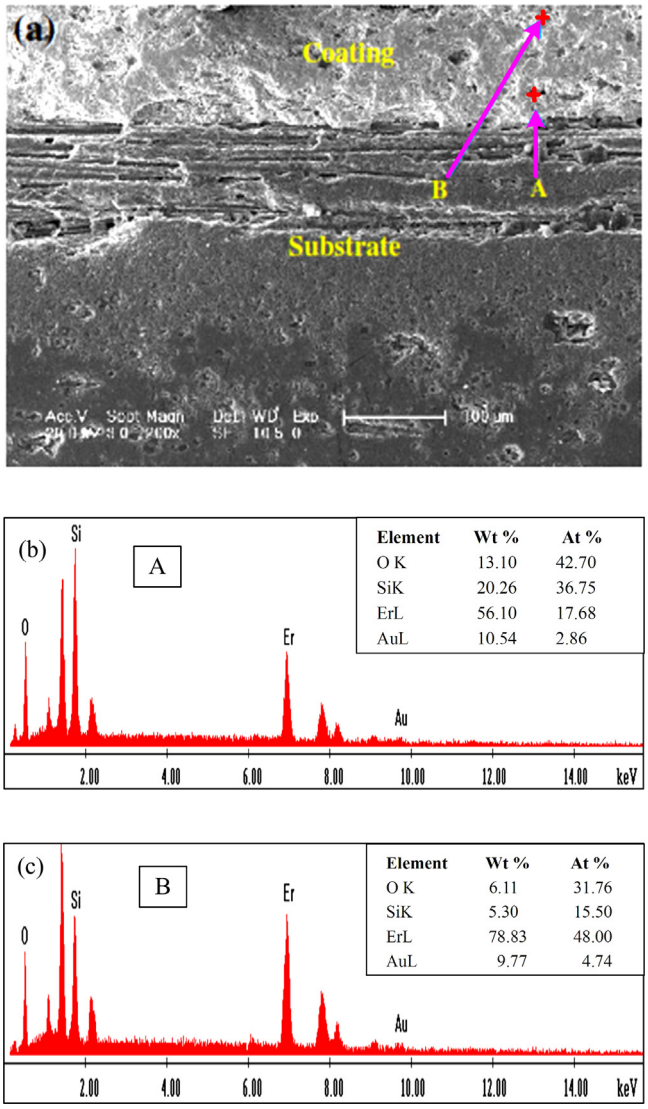

Fig. 6. (a) SEM image on the cross-section of the thermal cycled $Er_2Si_2O_7$ coating on C_f/SiC coupon and (b and c) EDS spectra along with elemental percentages for point A near the interface and point B near the surface, respectively.

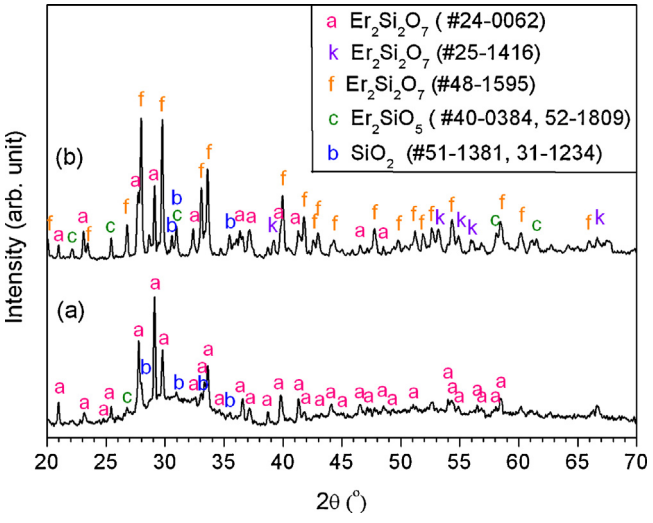

Fig. 7. XRD patterns of (a) as-sprayed $Er_2Si_2O_7$ coating and (b) the thermally cycled $Er_2Si_2O_7$ coating with 327 cycles with a flame temperature of 2000 °C. For each cycle, the coating was thermal cycled between surface temperatures of 400 °C and 1500 °C. (a) repeated for the sake of ease in comparison to the readers.

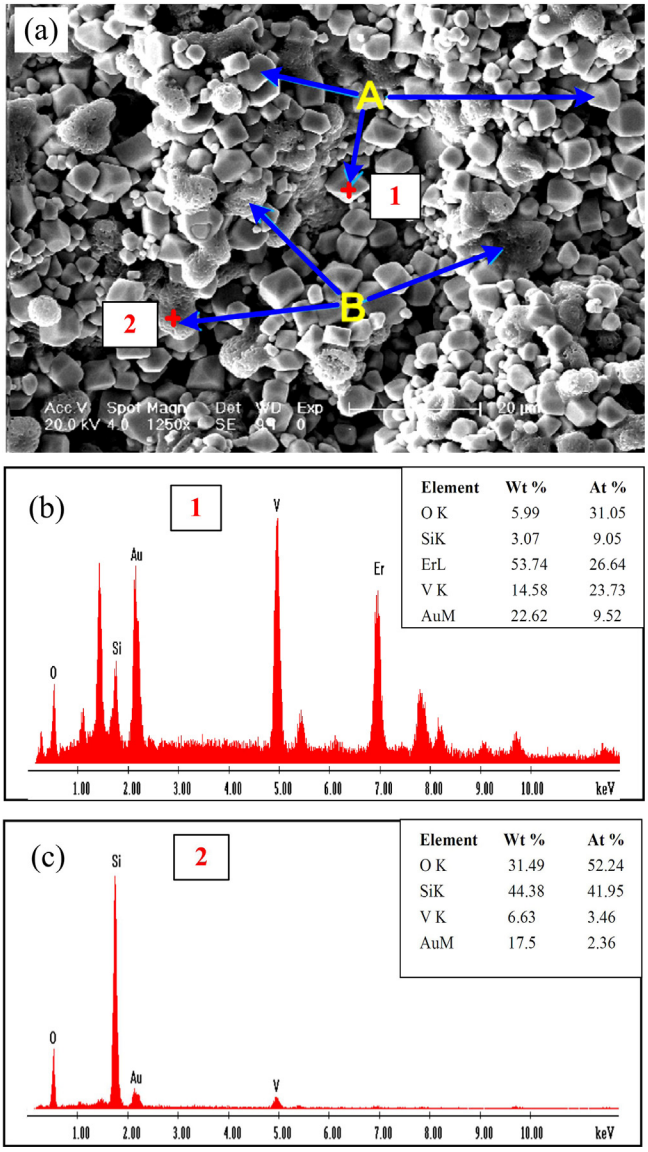

Fig. 8. (a) SEM image on the surface of plasma sprayed $Er_2Si_2O_7$ coating after exposure to molten V_2O_5 for 6 h at 800 °C and (b and c) EDS analysis for points 1 and 2 in (a), respectively.

thermal cycling. The Si proportion, on the other hand, has gone down in the surface region according to studies made by the EDS.

Microchemistry of coatings was also investigated further by the XRD that showed the occurrence of widespread structural transformations in the coating during thermal cycling between 400 °C and 1500 °C on a gas burner rig facility. For instance, $Er_2Si_2O_7$ with pdf card #24-0062 and with space group P21/b(14) has partially transformed into its disilicate versions with pdf cards #48-1595 (base center monoclinic structure) and 25-1416 (monoclinic with space group P21/c(14)). Meanwhile, the numbers of XRD peaks emanating from Er_2SiO_5 phase have also risen. The di-silicate versions existing in the thermal cycled coating have large density disparities, owing to which the cracking and subsequent failure in the coating might have occurred. Theoretical density of the newly formed $Er_2Si_2O_7$ phase (pdf card #48-1595) is 2.955 g/cc that is almost half than that for the originally deposited $Er_2Si_2O_7$ coating (pdf card #24-0062) with value 5.98 g/cc. The XRD pattern of transformed coating on thermal cycling between 400 °C and 1500 °C on gas burner rig facility is shown in Fig. 7.

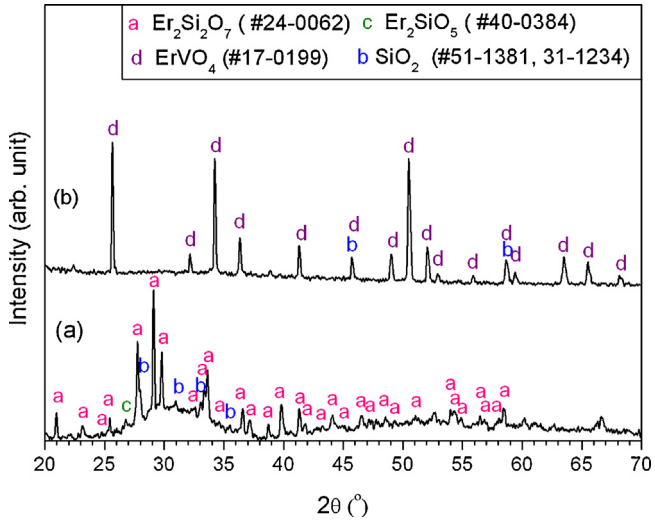

Fig. 9. XRD patterns of (a) the as-sprayed $Er_2Si_2O_7$ coating and (b) the coating after exposure to molten V_2O_5 salt for 6 h at 800 °C. (a) repeated again for the sake of ease in comparison to the readers.

3.4. Hot corrosion behavior of $Er_2Si_2O_7$ coating in molten vanadate salt

Fig. 8(a) shows the SEM surface morphology of the coating after exposure to molten vanadate salt for 6 h at 800 °C. It should be recalled that the V_2O_5 melts at 690 °C, and its density was reported to be 3.3 g/cc. On hot corrosion testing in vanadate salt, the coating surface was found with the presence of various new features. They include, for instance, the compact and sharp grains marked with letter "A" and the rounded and porous crystals marked with letter "B" with sizes 2–5 μm (Fig. 8(a)). Fig. 8(b) and (c) shows the element EDS spectra and corresponding quantitative analysis for point 1 and point 2, respectively. From the EDS results, the compact and sharp grains have significant proportions of vanadium implying that they are the reaction induced corrosion product; the rounded and porous crystals are also found with small quantities of vanadium, however with almost no signatures from the erbium. The results from the SEM/EDS were further verified by performing the XRD studies that revealed the large presence of a major corrosion product of $ErVO_4$ (Fig. 9). The possible interactions leading to formation of the vanadate based on erbium, i.e. $ErVO_4$ may be as follows:

$$Er_2Si_2O_7 + V_2O_5 = 2ErVO_4 + 2SiO_2 \quad (1)$$

Rare earth based orthovanadates such as $ErVO_4$ which has the crystal structure of tetragonal zircon type ($ThSiO_4$) have been widely studied from scientific and technological points of view. Meanwhile, the $ErVO_4$ is expected to be quite stable at the testing temperature used in our studies; with its melting temperatures reported to be 1680 °C [23,24]. The decomposition reaction of $Er_2Si_2O_7$ based on Eq. (1) also resulted in the formation of free SiO_2 that further enwraps in the vanadium containing melt. This process of rare earth orthovanadates and silica formation continues until the whole vanadium pentaoxide in the molten form is consumed. It would be important to mention that the original disilicate structure is no more existent and has undergone extensive transformation on hot corrosion testing. Combining SEM/EDS results (Fig. 8) with XRD analysis (Fig. 9), to our understandings, the compact and sharp grains marked with letter "A" are assigned to $ErVO_4$ and the rounded and porous crystals marked with letter "B" are silica (Fig. 8(a)).

4. Conclusions

$Er_2Si_2O_7$ powders were fabricated by the solid-state reaction of Er_2O_3 and SiO_2 powders in appropriate molar ratios. Some impurity peaks such as from Er_2SiO_5 have been observed after high temperature reaction synthesis. According to the dilatometric data, the average CTE value of $Er_2Si_2O_7$ from 150 °C to 1300 °C is calculated to be 4.3 ppm/°C. Atmospheric plasma spraying of the $Er_2Si_2O_7$ powders with spraying dried treatment was carried out on C_f/SiC coupons that resulted in the formation of well-distribution $Er_2Si_2O_7$ coatings. Gradient thermal cycling of the coated coupons between 400 °C and 1500 °C on a burner rig facility caused various kinds of transformations in the coating. The coating peeled off after total 327 thermal cycles, and the undergone cracking and structural transformations with known density disparities were found. Hot corrosion performance of the plasma sprayed $Er_2Si_2O_7$ coating investigated at 800 °C for 6 h in V_2O_5 revealed that the coating underwent severe transformations as a result of molten salt exposure, resulting in the destruction of original monoclinic $Er_2Si_2O_7$ structure and formation of $ErVO_4$ as a major reaction product due to leaching effects of corrodent.

Acknowledgements

This work is financially supported by the National Natural Science Foundation of China (51472235, 21171160, 51301180), the Chinese Academy of Sciences (CAS) Fellowships for Young International Scientist, Grant No. 2010Y1GA2 and the Higher Education Commission of Pakistan under NRPU.

References

[1] K.N. Lee, Protective Coatings for Gas Turbines. DOE-National Energy Technology Laboratory. http://www.netl.doe.gov/technologies/coalpower/turbines/refshelf/handbook/4.4.2.pdf (accessed 12.06.11).
[2] W. Krenkel and F. Berndt, Mater. Sci. Eng. A, 412, 177–181 (2005).
[3] W. Krenkel, Int. J. Appl. Ceram. Technol., 1, 188–200 (2004).
[4] J. Wang, M. Lin, Z. Xu, Y. Zhang, Z. Shi, J. Qian, G. Qiao and Z. Jin, J. Eur. Ceram. Soc., 29, 3091–3097 (2009).
[5] M. Pavese, P. Fino, C. Badini, A. Ortona and G. Marino, Surf. Coat. Technol., 202, 2059–2067 (2008).
[6] Y. Xiang, Z.H. Chen and F. Cao, J. Asian Ceram. Soc., 2, 305–309 (2014).
[7] P.D. Sarkisov, N.V. Popovich, L.A. Orlova and Y.E. Anan'eva, Glass Ceram., 65, 366–371 (2008).
[8] L.F. Cheng, Y.D. Xu, L.T. Zhang and R. Gao, Carbon, 38, 2133–2138 (2000).
[9] N.S. Jacobson, E.J. Opila and K.N. Lee, Curr. Opin. Solid State Mater. Sci., 5, 301–309 (2001).
[10] K.N. Lee, D.S. Fox and N.P. Bansal, J. Eur. Ceram. Soc., 25, 1705–1715 (2005).
[11] B.L. Zou, Z.S. Khan, X.Z. Fan, W.Z. Huang, L.J. Gu, Y. Wang, J.Y. Xu, S.Y. Tao, K.Y. Yang, H.M. Ma and X.Q. Cao, Surf. Coat. Technol., 219, 101–108 (2013).
[12] X.J. Wang, T. Nakajima, H. Isshiki and T. Kimura, Appl. Phys. Lett., 95, (2009), 041906–041906-3.
[13] M. Miritello, R.L. Savio, F. Iacona, G. Franzo, A. Irrera, A.M. Piro, C. Bongiorno and F. Priolo, Adv. Mater., 19, 1582–1588 (2007).
[14] R. Lo Savio, M. Miritello, A.M. Piro, F. Priolo and F. Iacona, Appl. Phys. Lett., 93, 021919 (2008).
[15] J. Wang, S. Tian, G. Li, F. Liao and X. Jing, Mater. Res. Bull., 36, 1855–1861 (2001).
[16] H.S. Tripathi and V.K. Sarin, Mater. Res. Bull., 42, 197–202 (2007).
[17] H. Wen, S. Dong, P. He, Z. Wang, H. Zhou and X. Zhang, J. Am. Ceram. Soc., 90, 4043–4046 (2007).
[18] D.D. Jayaseelan, S. Ueno, T. Ohji and S. Kanzaki, Mater. Chem. Phys., 84, 192–195 (2004).
[19] H. Chen, Y. Gao, Y. Liu and H. Luo, Inorg. Chem., 49, 1942–1946 (2010).
[20] Z.S. Khan, B.L. Zou, W.Z. Huang, X.Z. Fan, L. Gu, X.L. Chen, S.B. Zeng, C.J. Wang and X.Q. Cao, Mater. Sci. Eng. B, 177, 184–189 (2012).
[21] X.Q. Cao, R. Vassen, W. Fischer, F. Tietz, W. Jungen and D. Stover, Adv. Mater., 15, 1438–1442 (2003).
[22] Z.S. Khan, B.L. Zou, X.L. Chen, C.J. Wang, X.Z. Fan, L.J. Gu, W.Z. Huang and X.Q. Cao, Surf. Coat. Technol., 207, 546–554 (2012).
[23] O.N. Ustalova, G.A. Rykova, V.M. Skorikov and I.V. Tananaev, Russ. J. Inorg. Chem., 23, 1733–1736 (1978).
[24] K. Oka, H. Unoki, H. Shibata and H. Eisaki, J. Cryst. Growth, 286, 288–293 (2006).